ACS OMEGA

http://pubs.acs.org/journal/acsodf

Article

Highly Efficient Photocatalytic Degradation of Tetracycline by Modifying UiO-66 via Different Regulation Strategies

Xu Jia, Fuying Wang, Xuetong Xu, Cong Liu, Liuxue Zhang,* Shuyan Jiao,* Genxing Zhu, Xiulian Wang, and Guomin Yu

Cite This: *ACS Omega* 2023, 8, 27375−27385

Read Online

ACCESS | Metrics & More | Article Recommendations | Supporting Information

ABSTRACT: Wastewater containing organic pollutants cause potential harm to the environment and human health. A series of zirconium-organic frameworks (UiO-66) and their composites were synthesized by solvothermal methods, including band gap adjustment, heterojunction construction, and metal ion doping. For the model pollutant tetracycline (TC), all of the prepared catalysts could achieve effective degradation of it. Therein, the degradation efficiency of tetracycline could reach 95% under the UV irradiation with the aid of the catalyst, in which the UiO-66-NDC was modified with P−C_3N_4. The free radical capture experiments demonstrated that the superoxide radical ($^{\bullet}O_2^-$) was the main oxidizing species for the photodegradation of tetracycline. Hence, the improvement strategy of the catalyst would provide some enlightenment for the development of more efficient photocatalysts for the degradation of organic dyes in wastewater.

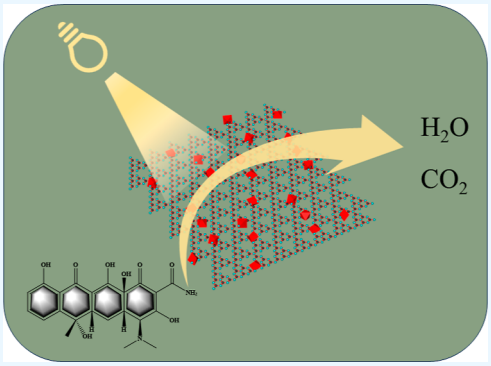

1. INTRODUCTION

In recent years, due to the expanding demand of medicine and pigment printing and dyeing industry, a large amount of chemical wastewater containing organic dyes has been produced, which creates the problem of organic pollutants harming human life.[1] Many physical and chemical technologies have been developed for the treatment of wastewater, such as membrane filtration,[2] Fenton oxidation,[3] biological treatment,[4] and adsorption,[5] However, most dye molecules possessed large conjugated structures that cannot be completely removed, and had disadvantages such as low efficiency, high cost, and secondary pollution. Photocatalysis technology could produce strong oxidizing free radicals under light conditions and completely degrade organic pollutants into CO_2, H_2O, and inorganic salts, without secondary pollution. Therefore, the development of efficient photocatalytic technology to degrade organic dyes in wastewater has been considered as an important task for a sustainable society.

Metal−organic frameworks (MOFs) are a new class of coordination porous crystalline materials formed by self-assembling organic ligands with metal ions, which are characterized by high specific surface area, multiple active sites, diverse structures, tailorability, and easy functionalization.[6] However, due to the unstable structure, small specific surface area, and wide band gap of the initial MOFs, their application in the field of photocatalysis was limited. Therefore, researchers have tried to practice different methods to modify MOFs to improve their application value. Compared with single metal materials, the synergistic effect of mixed metals in MOFs was used to enhance the flexibility of the photocatalytic materials, and the photocatalytic performance was significantly enhanced. Cui group synthesized the Cu-Doped MIL-101(Fe) as photocatalytic materials through the traditional solvothermal method, and the photocatalytic performance for tetracycline hydrochloride (TC) was more than 93% within 120 min.[7] Due to the introduction of Co(II) sites into the MOFs, the photogenerated ROS type changed from the initial single linear oxygen ($^1O_2$) to multiple ROS ($^1O_2$ and $^{\bullet}O_2^-$), where $^{\bullet}O_2^-$ is the main active substance for the degradation rate of tetracycline.[8] In addition, by using some ligands with larger conjugated systems to regulate the band gap and increase the pore size and specific surface area of the materials, we could also improve the photocatalytic performance of the MOFs. Yulia et al. used 2,6 naphthaladiate (NDC) ligand to replace 1,4 phthalic acid (BDC) ligand in the traditional reaction to synthesize Cr-MOF materials with better performance.[9] Changing substituents also could regulate the chemical microenvironment the of MOFs efficiently.[10] Wang group synthesized a series of MIL-101-X with various substituents (−H, $-NH_2$, −OH, and $-OCH_3$), which substantially improve its removal efficiency of refractory

Received: April 22, 2023
Accepted: July 12, 2023
Published: July 24, 2023

ACS Publications

© 2023 The Authors. Published by American Chemical Society

pollutants in the Fenton-like reaction via the introduction of various substituents into the side chain of MIL-101(Fe).[11] Moreover, the construction of the heterojunction could also improve the photocatalytic performance of MOFs. He et al. prepared an In_2S_3/MIL-100(Fe) heterojunction by the solvothermal method, the removal efficiency of tetracycline hydrochloride was increased sharply, which indicated the powerful combination of MOFs, and the semiconductor was a promising approach to fabricate a heterojunction photocatalyst for wastewater purification.[12] g-C_3N_4 is a metal-free semiconductor, which is an outstanding photocatalyst due to its special π-conjugated electronic structure, narrow band gap, good stability, and easy synthesis route. g-C_3N_4 has been widely applied in many fields.[13]

Hence, a series of photocatalysts based on the classical Zr-MOF UiO-66 modified by incorporating other metals, constructing heterojunctions, and changing ligands were synthesized. Among them, due to the strong affinity of carboxylate and Zr(IV) cations,[14] the UiO-66 possessed better thermal and chemical stability. The larger conjugated systems of 1,4 naphthalene dicarboxylic acid (NDC) enabled the MOF to have a larger surface area and porosity that was conducive to the adsorption of organic pollutants. The heterojunction constructed by the protonated g-C_3N_4 could improve the electron migration rate and degradation efficiency. By employing these different modification schemes, some helpful inspiration could be provided for the design of photocatalysts with high activity.

2. EXPERIMENTAL SECTION

2.1. Materials and Synthesis. Zirconium tetrachloride (AR) was obtained from Guangdong Wong Jiang Chemical Reagent Co., Ltd. 1,4-naphthalenedicarboxylic acid (95%), terephthalic acid (99%), and cobalt chloride hexahydrate ($CoCl_2{\cdot}6H_2O$) (AR) were obtained from Zhengzhou Alfa Chemical Co., Ltd. Tetracycline hydrochloride (96%) and melamine (99%) were purchased from Shanghai Macklin Biochemical Co., Ltd. Rhodamine B (RhB) (BS), methyl orange (MO) (IND), ascorbic acid (AR), and disodium edetate (AR) were obtained from Tianjin Guangfu Technology Development Co., Ltd. All chemicals and reagents used were analytically pure and could be used without further purification.

2.1.1. Synthesis of UiO-66 and UiO-66-NDC. UiO-66 was synthesized according to the traditional solvothermal method reported in previous literature.[15] $ZrCl_4$ (0.1864 g, 0.80 mmol) and terephthalic acid (H_2BDC) (0.1449 g, 0.87 mmol) were dissolved in 16 mL of *N*,*N*-dimethylformamide (DMF) ultrasonically for 0.5 h to disperse evenly, and then, 96 μL of hydrofluoric acid was added. After that, the solution was transferred to a Teflon-lined stainless-steel reactor and maintained at 150 °C for 24 h. The products were collected by centrifugation and washed with DMF and methanol several times, respectively. The products were dried in an oven at 70 °C overnight and named UiO-66. As a comparison, terephthalic acid was replaced with 1,4-naphthalene dicarboxylic acid (0.1729 g, 0.80 mmol) as the organic ligand coordinated with Zr^{4+} in the process of synthesis. The experimental procedure was the same as that for the above operation, and the product was named UiO-66-NDC.

2.1.2. Synthesis of Co/UiO-66-NDC. The cobalt ion doped UiO-66-NDC was synthesized by referring to the previous reports.[16] Briefly, zirconium tetrachloride (0.1864 g, 0.80 mmol) and cobalt chloride hexahydrate (0.1183 g, 0.80 mmol) are dissolved in 15 mL of DMF organic solvent; after stirring evenly, 1,4-naphthalenedicarboxylic acid (0.3458 g, 1.60 mmol) was added and stirred again for 1 h. After that, the mixed solution was transferred to a Teflon-lined stainless-steel reactor and maintained at 120 °C for 24 h. After the reaction was finished, the slurry was centrifuged at 12,000 rpm for 3 min, the solid product was washed with ethanol several times, and finally dried at 70 °C overnight, named Co/UiO-66-NDC.

2.1.3. Synthesis of g-C_3N_4. g-C_3N_4 was prepared following the previous report.[17] Typically, 10 g of melamine was put into a quartz boat and then heated to 550 °C for 4 h in a tube furnace (heating rate of 2 °C min^{-1}), and the bulk g-C_3N_4 yellow powder was obtained.

2.1.4. Synthesis of P−C_3N_4. The protonated g-C_3N_4 was prepared by chemical stripping. The blocky g-C_3N_4 sample (0.4 g) was dispersed in 20% HNO_3 aqueous solution and stirred at room temperature for 6 h. Then, the solution was transferred to a Teflon-lined stainless-steel reactor and maintained at 150 °C for 2 h. Naturally cooling to room temperature, the slurry was centrifuged at 12,000 rpm for 3 min. The obtained product was washed with water several times to neutrality, dried at 70 °C for 12 h in a vacuum oven, and denoted by P−C_3N_4.

2.1.5. Synthesis of UiO-66-NDC/P−C_3N_4. UiO-66-NDC/P−C_3N_4 was synthesized by a solvothermal process. 0.0145 g of P−C_3N_4 was dispersed in 10 mL of DMF and ultrasonicated for 10 min. Then, 0.058 g of zirconium tetrachloride and 0.044 g of 1,4-NDC were added into the above dispersion under continuous stirring, and ultrasonic treatment was carried out again for 30 min. Subsequently, the mixture was retained at 150 °C for 24 h in a Teflon-lined stainless-steel autoclave. After the reaction is finished, the slurry was centrifuged at 12,000 rpm for 3 min, the lower solid was washed with absolute ethanol many times, and then, the sample was dried at 70 °C for 12 h in a vacuum oven and named UiO-66-NDC/P−C_3N_4.

2.2. Characterization. The structure of functional groups on the surface of the material was analyzed by a Fourier infrared spectrometer (FTIR, Nicolet iS50, USA). The surface morphologies of the samples were studied by scanning electron microscopy (SEM, Phenom, Netherlands). The crystal structures of photocatalyst samples were determined by X-ray diffraction (XRD, Ultima IV, Japan) and Cu K irradiation was used. The surface composition and chemical environment were analyzed by X-ray photoelectron spectroscopy (XPS, Axis Ultra, Japan). The electronic and optical properties of UiO-66-NDC/P−C_3N_4 were studied by Mott−Schottky (Electrochemical Work, CHI660, Shanghai) and UV−vis DRS (Shimadzu UV-2600) tests. The carrier migration efficiency of UiO-66-NDC/P−C_3N_4 was investigated and analyzed by fluorescence spectroscopy (PL) (Hitachi F-7100).

2.3. Characteristics Conditions of Photocatalytic Degradation. The photocatalytic properties of UiO-66, UiO-66-NDC, Co/UiO-66-NDC, and UiO-66-NDC/P−C_3N_4 composites were studied by photodegradation of tetracycline. Twenty milliliters of tetracycline solution (30 mg/L) was accurately pipetted into the reaction tube, and the absorbance value (C_0) was determined by a UV-spectrophotometer (500 W). A certain amount of composites was added into the solution, and stirred for 1 h in the dark condition at room temperature to reach the adsorption/desorption equilibrium. Then, the solution was degraded in a multifunc-

https://doi.org/10.1021/acsomega.3c02762
ACS Omega 2023, 8, 27375−27385

tional photochemical reactor (SGY-II) equipped with a 500 W xenon lamp under the irradiation wavelength of 420 nm. The real-time absorbance value (C_t) of the solution was tested for 20 min.

3. RESULTS AND DISCUSSION

3.1. Structure Characterization. The crystal structure of the photocatalyst samples under different modification methods was determined by powder X-ray diffraction (XRD). As shown in Figure 1, the diffraction peaks at 2θ =

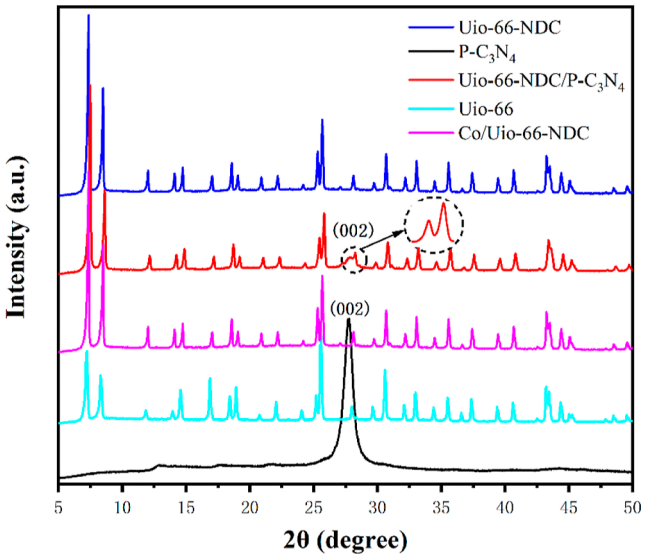

Figure 1. X-ray diffraction contrast diagram of the photocatalyst sample

7.56, 8.58, and 25.82 could be observed from the XRD pattern of UiO-66, which correspond to the (111), (200), and (600) crystal faces of UiO-66, respectively.[18] As illustrated in Figure 1, when the terephthalic acid was replaced by the 1,4-naphthalenedicarboxylic acid, the peak intensity corresponding to the diffraction peak in the corresponding XRD pattern changed obviously. The difference of diffraction peak intensity might be caused by the different grain sizes, and it also proved that the substitution of ligand could not affect the stable crystal structure of Zr-MOF. According to the Scherrer formula,[19] the crystal size of (111) crystal face changed from 39.85 to 79.91, and the crystal size of the (002) crystal face changed from 44.3 to 66.47. The crystal size of the (600) crystal face changed from 58.25 to 62.79, indicating that the difference of diffraction peak intensity was caused by the changes of crystal size. When the heterojunction was constructed by the P−C_3N_4 and UiO-66-NDC/P−C_3N_4, the sharp diffraction peak at 2θ = 27.8 corresponding to the (002) crystal plane appeared. This strong peak was the interlayer stacking characteristic in aromatic compounds and might be caused by the destruction of the in-plane structure of aromatic heterocyclic triazine and the breakage of the hydrogen bond in the protonation process. The peak at 12.8 [(100) crystal plane] almost disappeared. This phenomenon illustrated that the protonated P−C_3N_4 was prepared successfully and the heterojunction of UiO-66-NDC and P−C_3N_4 was constructed without the destruction of the crystal structure of UiO-66-NDC. This result indicated that the composite catalyst would possess a higher efficiency to the use of light and then improve the degradation efficiency of the organic pollutant. In addition, when the cobalt ions were doped into UiO-66-NDC, the crystal structure of UiO-66-NDC remained stable. The stable structure of the catalyst helped them play an important role in the field of photocatalytic degradation of pollutants.

The structural information on these photocatalysts could also be obtained by infrared spectroscopy. As shown in Figure S1, the absorption peaks of UiO-66 samples at 1589, 1396, and 746 cm^{-1} were, respectively, attributed to the "in-phase stretching", "symmetric vibration", and "C−H vibration" of the carboxylate (−COOH) group in their ligand terephthalic acid.[20,21] However, the strong vibrational bands at 1419 and 1460 cm^{-1} observed in the infrared spectrum of UiO-66-NDC (Figure S1b) can belong to the characteristic backbone vibration of the naphthalene ring in the 1,4-naphthalenedicarboxylic acid ligand. Interestingly, the peaks at 1367 and 1657 cm^{-1} represent symmetric and asymmetric vibration peaks of the carboxylate ion (COO−), respectively, suggesting that the 1,4-naphthaleneate ligand lost its proton and binds to Zr^{4+} to form MOF.[22] Besides typical absorption of the UiO-66-NDC, the characteristic absorption peaks of P−C_3N_4 could also be observed in the spectrum of the composite UiO-66-NDC/P−C_3N_4, such as the C−N heteroring expansion vibration peak at 1200−1650 cm^{-1} and the typical mode representing the triazine unit at 810 cm^{-1}. This result indicated that the heterojunction was successfully prepared. Compared with UiO-66-NDC, the infrared spectrum of Co/UiO-66-NDC in Figure S1c was basically unchanged, indicating that the doping of cobalt ions did not change its stable chemical structure.

The morphology of the catalysts could be observed in the SEM. As shown in Figure 2a,b both UiO-66 and UiO-66-NDC showed an octahedral morphology similar to existing studies in the literature.[23,24] Short petal-like structures of the P−C_3N_4 could be observed in Figure 2c. It was worth noting that not only the UiO-66-NDC appears as octahedra after the loaded protonated P−C_3N_4, but the presence of both species could be clearly observed (Figure 2d). When the UiO-66-NDC was modified with cobalt ions, the morphology stayed the same and the dispersion was improved (Figure 2e). The results of TEM images were consistent with the results of SEM (Figure 2f−i).

The composition and surface elements state of these materials could be obtained from XPS (Figure 3). The occurrence of major characteristic peaks of Zr 3d, C 1s, N 1s, and O 1s at 183.4, 286, 400.1, and 532 eV, respectively, indicated that the corresponding elements existed in the catalysts UiO-66 (C, O), UiO-66-NDC (C, O), P−C_3N_4 (C, N), UiO-66-NDC/P−C_3N_4 (C, N, O), and Co/UiO-66-NDC (C, O). Figure 3c shows the high-resolution C 1s comparison of the catalyst. The peaks at 284.8 and 288.0 (288.3) eV belonged to the standard carbon signal (C−C) and the graphitic phase structure (P−C_3N_4) with sp_2 hybrid carbon atom (N−C═N) signals, respectively. The peak at 288.7 (288.8) eV was caused by the C═O of the carboxylic acid group in the MOF ligand.[25,26] The weak peak at 285.8 (285.7, 285.5) eV represented the C−O bond in the organic ligand.[26] The shift of the peak might be caused by the chemical environment change of the carbon atoms.

By fitting the N 1s high-resolution spectrum of P−C_3N_4 (Figure 3d), three main peaks belonging to different components could be obtained. The peak at 398.5 (398.8) eV was attributed to the combination of an aromatic N atom

https://doi.org/10.1021/acsomega.3c02762
ACS Omega 2023, 8, 27375−27385

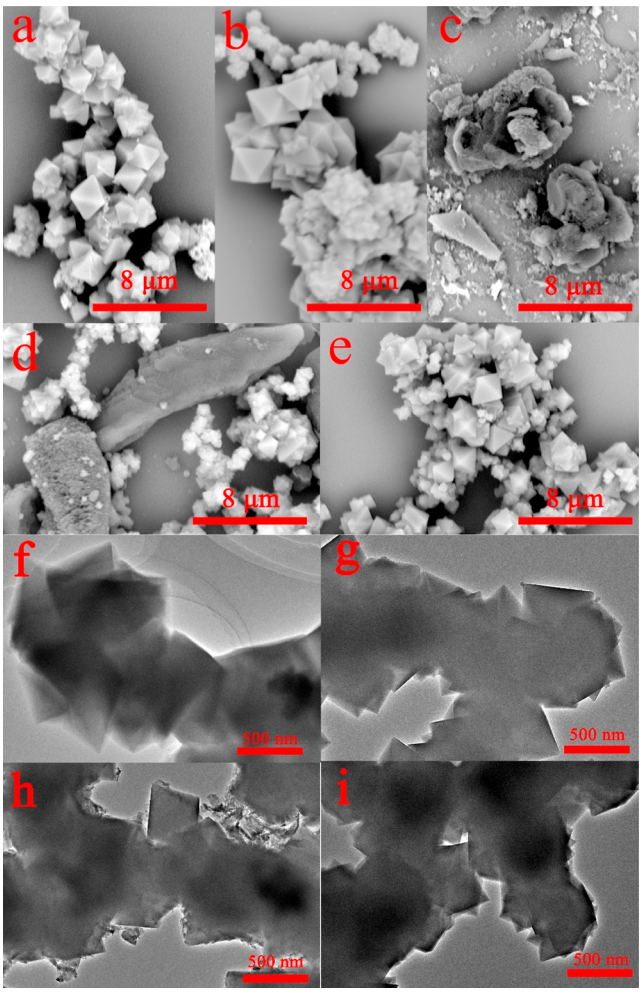

Figure 2. SEM images of the photocatalyst sample: (a) UiO-66, (b) UiO-66-NDC, (c) P−C_3N_4, (d) UiO-66-NDC/P−C_3N_4, and (e) Co/UiO-66-NDC. TEM images of the photocatalyst sample: (f)UiO-66, (g) UiO-66-NDC, (h) UiO-66-NDC/P−C_3N_4, and (i) Co/UiO-66-NDC.

with two C atoms in the triazine or heptazine ring (C−N═C). The peak binding energy of the N−$(C)_3$ group was 400.4 (400.6) eV. In addition, the weak peak observed at 404.0 (404.2) eV represents N($-NH^+$) with a positive charge effect, which proved the protonation of P−C_3N_4.[27] Compared with P−C_3N_4, the corresponding peak positions of C 1s and N 1s in UiO-66-NDC/P−C_3N_4 shifted to the higher binding energy caused by the redistribution of electrons after the formation of the heterojunction, which confirmed the transfer of electrons from P−C_3N_4 to UiO-66-NDC after recombination. By fitting the O 1s of UiO-66-NDC and Co/UiO-66-NDC, respectively (Figure 3e), three peaks related to the Zr−O/Co−O bond (532.6 eV), C═O bond (531.5 eV), and O−H bond (530.6 eV) were acquired,[28] which proved that the cobalt was successfully doped into UiO-66-NDC. The peaks at the binding energies of 782.4 and 796.6 eV represented Co $2p_{3/2}$ and Co $2p_{1/2}$ in the high-resolution fitting diagram of Co 2p (Figure 3f), respectively, which indicated that the doped Co element was connected with the O atom to form the Co−O bond in the catalyst Co/UiO-66-NDC.[29]

3.2. Photoelectric Characteristics. The transport efficiency of the carrier was investigated and analyzed by steady-state photoluminescence (PL). A weak emission peak intensity indicated a low photogenic hole-charge recombination rate. In the fluorescence emission spectra (Figure 4a), it could be observed that the UiO-66-NDC/P−C_3N_4 catalyst exhibited a weaker broad peak compared with UiO-66-NDC. This result indicated that the heterojunction could effectively accelerate the separation of photogenerated carrier, reduces the photogenerated hole and electron recombination rate, provide more oxidation active sites in the system. The UiO-66-NDC/P−C_3N_4 might show a better photocatalytic degradation performance. The same result was also reflected in the electrochemical impedance spectroscopy (Figure 4b). The Nyquist chart radius of UiO-66-NDC/P−C_3N_4 composites was significantly reduced compared to that of UiO-66-NDC, which meant that the electronic resistance of the composites was smaller. These above-mentioned results indicated that the construction of heterojunction could improve the separation and migration of photogenerated charge carriers.[30]

The photoresponse range and energy band of the catalyst depended on the electronic structure (Figure 4c). When the ligand was changed from terephthalic acid to 1,4-naphthalene dicarboxylate, the absorption range shifted from the ultraviolet region to the visible region, which indicated that the UiO-66-NDC might possess the ability to degrade pollutants under visible light. In addition, the band gap value of semiconductor catalysts was an important optical property used to evaluate photogenerated hole-charge formation. The E_g values of photocatalysts UiO-66 (2.6 eV) and UIO-66-NDC (2.38 eV) were obtained by calculation (Figure 4d). The decrease of the band gap value was attributed to the higher conjugated degree of 1,4-naphthalene dicarboxylate, which was more closely arranged relative to each other. Compared with terephthalic acid, the 1,4-naphthalene dicarboxylate as a ligand showed a higher degree of delocalization, more uniform charge density distribution, and lower absorbed energy by the $\pi-\pi^*$ transition.[31] Therefore, the catalyst using a greater conjugated system as a ligand had unique advantages in the field of visible light catalysis.

The electronic band structure information on the UiO-66-NDC/P−C_3N_4 was investigated by the Mott−Schottky analysis (Figure 4f). The positive slope of the Mott−Schottky curve reflected that the catalyst was a typical N-type semiconductor, and the flat band potential was −0.26 eV by estimation. For the N-type semiconductor, the conduction band potential was 0.1 eV lower than the flat charged potential, so it could be calculated that the conduction band potential of this catalyst was −0.36 eV.[32]

3.3. Experimental Performance Analysis of Photocatalysis. *3.3.1. Photocatalytic Properties of Different Catalysts.* The catalysts were prepared via three means of modification based on the UiO-66, which were ligand replacement, heterojunction construction, and incorporation of cobalt ions. The improvement of photocatalytic performance was evaluated by comparing the ability of four photocatalytic materials to deactivate tetracycline under visible light. As illustrated in Figure 5, the photocatalytic degradation rates of UiO-66-NDC, UiO-66-NDC/P−C_3N_4, and Co/UiO-66-NDC with a mass of 10 mg reached 52, 95, and 74%, respectively, for 30 mg/L tetracycline within 120 min, while the degradation rate of UiO-66 was only 26% under the same conditions. Compared with UiO-66, UiO-66-NDC had a lower band gap, a larger visible light absorption range, and a higher light utilization. The heterojunction constructed by the UiO-66-NDC and P−C_3N_4 improved the separation efficiency of

https://doi.org/10.1021/acsomega.3c02762
ACS Omega 2023, 8, 27375−27385

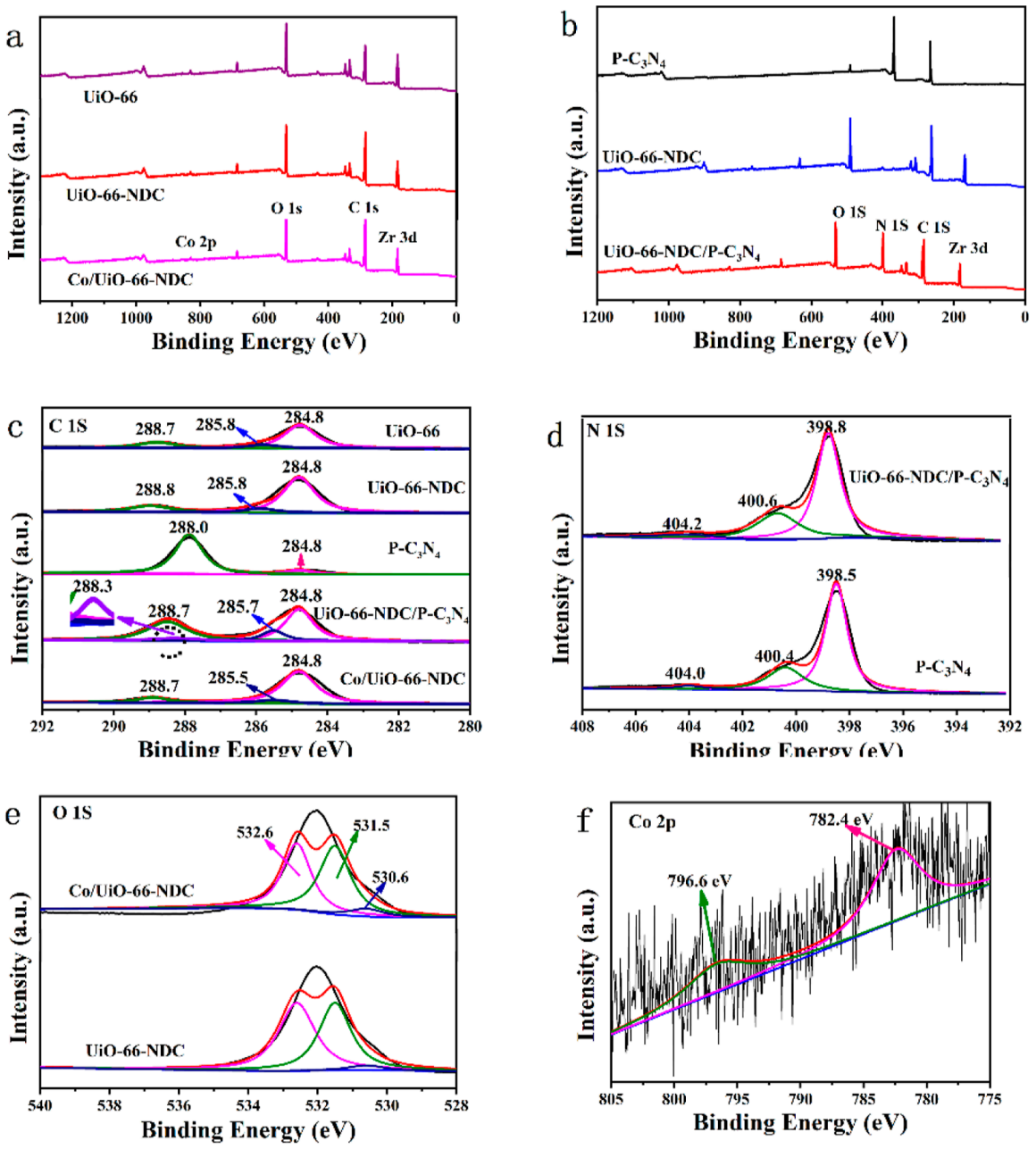

Figure 3. XPS comparison spectrum of photocatalytic samples: (a) XPS full spectrum, (b) XPS full spectrum, (c) C 1s, (d) N 1s, (e) O 1s, and (f) high-resolution fitting diagram of Co 2p.

the photogenerated hole charge. Due to the synergistic effect of cobalt and zirconium bimetallic ions, Co/UiO-66-NDC possessed a higher activity. All the catalysts modified by the above-mentioned schemes showed a better photocatalytic performance than the substrate UiO-66. Therein, the UiO-66-NDC/P−C_3N_4 possessed an optimal photocatalytic activity and the highest degradation rate. Consequently, UiO-66-NDC/P−C_3N_4 was selected as the representative catalyst to study the photocatalytic degradation performance of tetracycline.

3.3.2. Photocatalytic Performance with Different Amounts of Catalyst. The appropriate amount of catalyst had an important influence on the catalytic performance. Tetracycline was selected as a pollutant model, and the photocatalytic performance with different amounts of catalyst was discussed in the antibiotic solution with the concentration of 40 mg/L. As shown in Figure 6a, the degradation efficiency of tetracycline gradually increased with the increase of the amount of catalyst. This mainly because the active sites increased with the increase of the electrons and holes.[33] However, when the mass of the catalyst was further increased to 12 mg, the photocatalytic degradation effect was decreased, which was attributed to the fact that the catalyst dispersion was affected when the system contained an excessive amount of catalyst powder, impeded the interaction between the visible light and catalyst, and decreased the utilization rate of light while reducing the light penetration utilization.[34]

3.3.3. Photocatalytic Performance with Different Initial Concentrations. In order to explore the appropriate concentration of pollutant, different initial concentrations of the tetracycline solutions were selected to investigate the trend of the degradation degree in the presence of UiO-66-NDC/P−

https://doi.org/10.1021/acsomega.3c02762
ACS Omega 2023, 8, 27375−27385

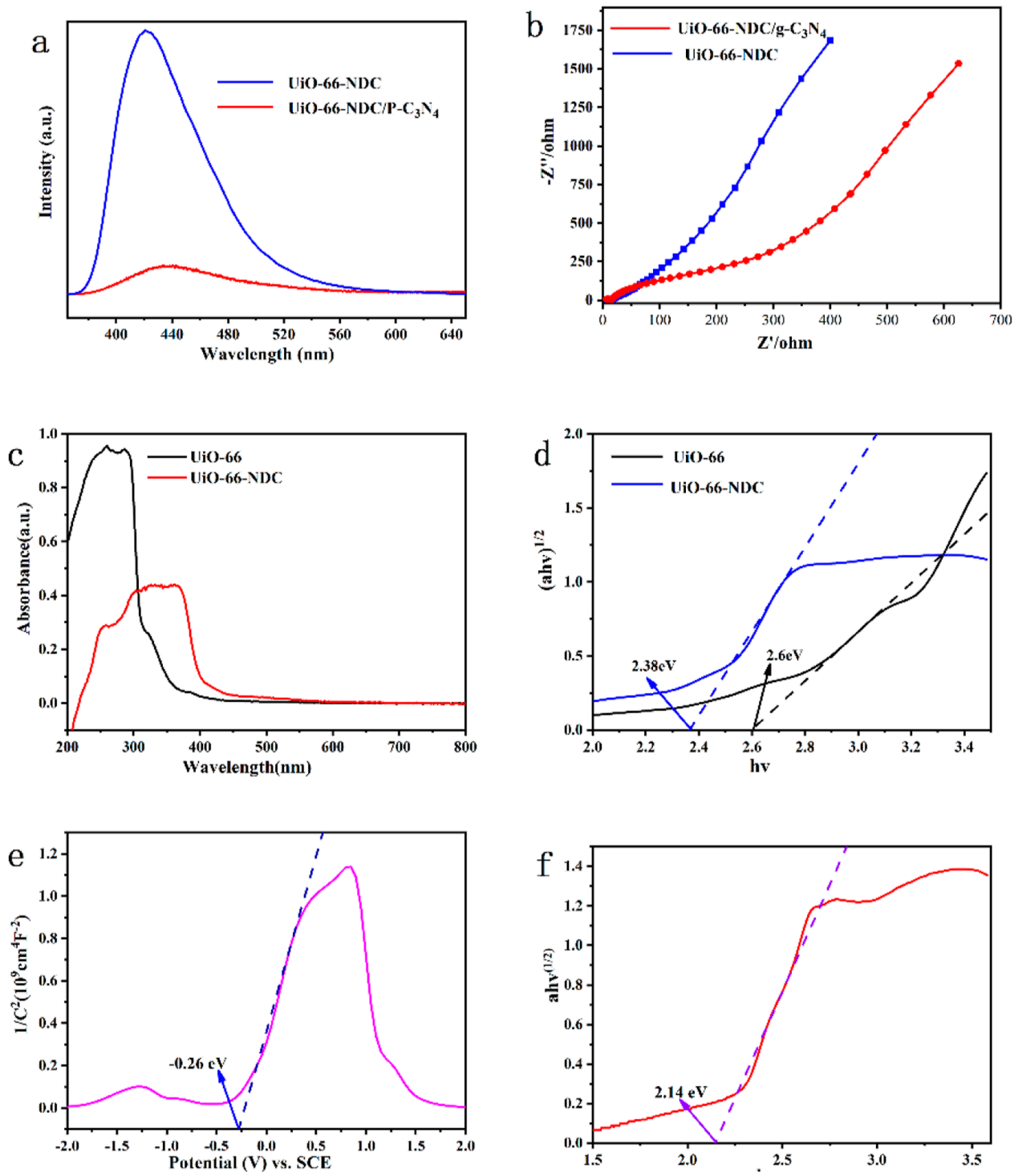

Figure 4. (a) PL, (b) electrochemical impedance, (c) UV−vis DRS, (d) band gap diagram of UiO-66 and UiO-66-NDC, and the (e) band gap diagram. (f) Mott−Schottky plots of UiO-66-NDC/P−C_3N_4.

C_3N_4 under visible light. It could be clearly observed that the degradation effect gradually decreased with an increase of the tetracycline concentration in Figure 6b. This phenomenon was caused by the obvious competition between the additional intermediates and the undegraded TC molecules in solution as the pollutant concentration increases,[35] and the decrease of the free radicals leading to the cover of catalyst surface by the tetracycline molecules and intermediates.[36,37]

3.3.4. Photocatalytic Performance with Different Types of Coexisting Ion. In order to investigate the effect of coexisting ions in the solution, the tetracycline solution (40 mg/L) with NaCl, $NaHCO_3$, $MgCl_2$ and Na_2SO_4 (0.05 mol/L), respectively, was degraded by the UiO-66-NDC/P−C_3N_4 under the visible light. The effects of HCO_3^- and SO_4^{2-} on the photocatalytic activity were investigated using Na^+ as the cation. As illustrated in Figure 6c, when HCO_3^- was added in the solution, only 14.4% of the sample was degraded under the

https://doi.org/10.1021/acsomega.3c02762
ACS Omega 2023, 8, 27375−27385

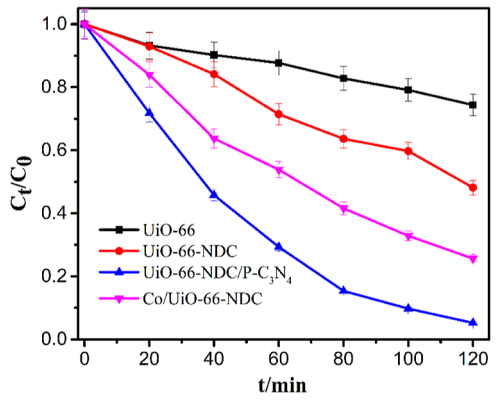

Figure 5. Effects of different photocatalyst types on tetracycline degradation.

same condition. As HCO_3^- would hydrolyze to CO_3^{2-}, which was an active substance quencher, the degradation of the pollutant was inhibited. For the HCO_3^-, active species h^+ and $^{\bullet}OH$ could react with HCO_3^- and CO_3^{2-} to generate a carbonate radical ($CO_3^{-\bullet}$). However, the oxidation capacity of $CO_3^{-\bullet}$ is extremely weak, leading to a significant decrease in photocatalytic degradation of TC.[38,39] h^+ and $^{\bullet}OH$ also consumed to produce sulfate radicals ($SO_4^{-\bullet}$). $SO_4^{-\bullet}$ are also less oxidizing than h^+ and leads to a decrease in photocatalytic efficiency. In addition, anions could compete with TC to occupy active sites and thus inhibit photocatalytic activity.[39,40] In particular, the effects of Mg^{2+} and Na^+ on photocatalytic activity were investigated by using Cl^- as the anion. It could be found that the degradation of tetracycline was increased in the presence of both Mg^{2+} and Na^+. The tetracycline was completely degraded within 60 min in the presence of Mg^{2+}, which implied Mg^{2+} could possess higher TC binding capacity than UiO-66-NDC/P−C_3N_4.[41] Or it might occur as the result of the stronger binding of bivalent cation to UiO-66-NDC/P−C_3N_4 than TC. For example, a monovalent cation only occupied one adsorption site on the surface of UiO-66-NDC/P−C_3N_4, while Mg^{2+} captured two empty seats and limited the adsorption of TC molecules.[42]

3.3.5. Recycling Performance Study. The recyclability of catalysts was an important factor used to evaluate whether they could be widely used for practical applications. Therefore, it was necessary to further investigate the reusability of

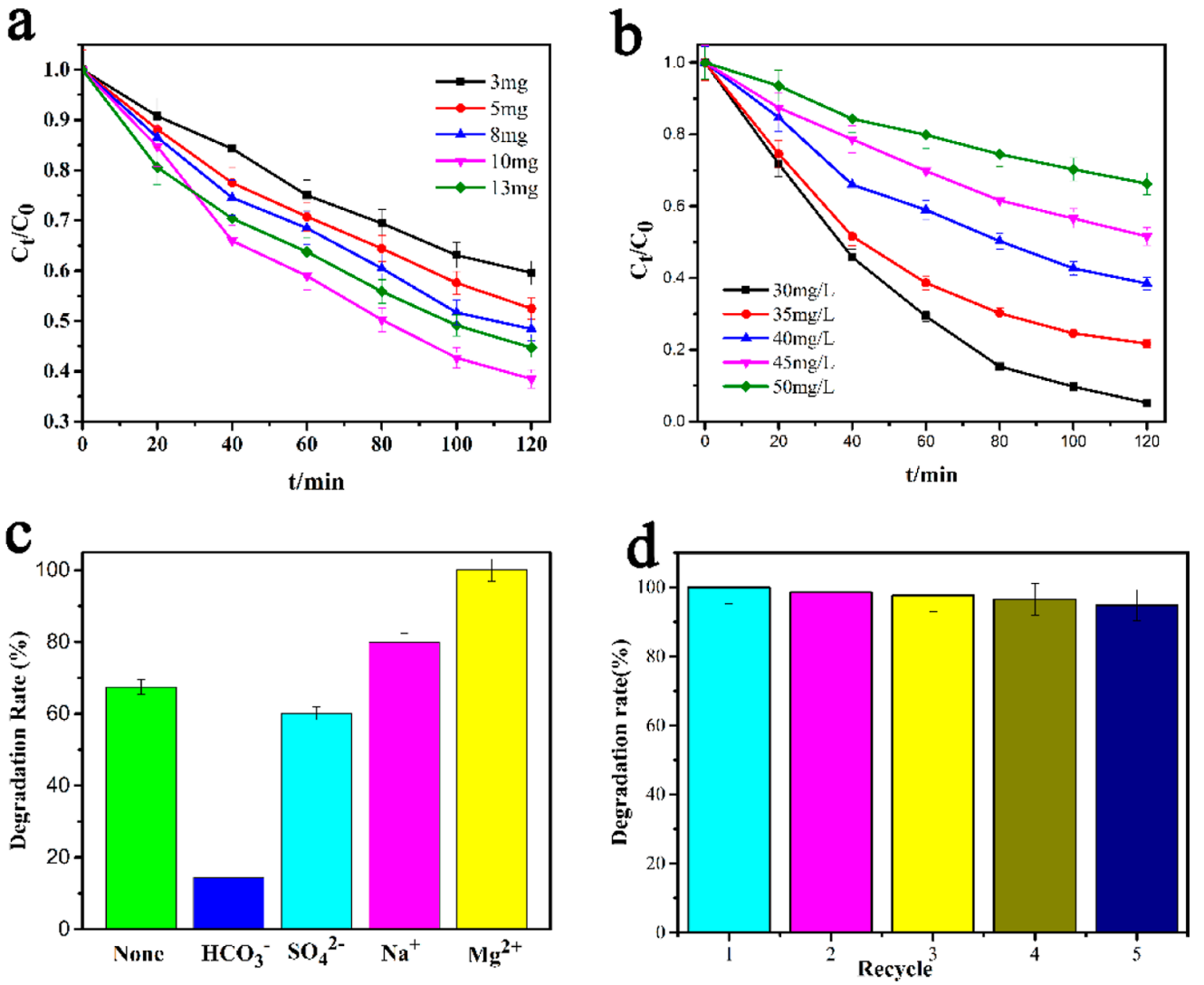

Figure 6. Effects of (a) different qualities, (b) initial pollutant concentration, (c) coexistence of different ions, and (d) the recycling performance on tetracycline degradation with the UiO-66-NDC/P−C_3N_4.

https://doi.org/10.1021/acsomega.3c02762
ACS Omega 2023, 8, 27375−27385

photocatalysts. The catalytic performance of UiO-66-NDC/P−C_3N_4 was investigated by several cyclic experiments (Figure 6d). The degradation efficiency of tetracycline was decreased from 95 to 87%. The UiO-66-NDC/P−C_3N_4 after repeated catalytic reactions was characterized by the infrared spectra and XRD, and the result showed that the catalyst could still maintain its structure well after recycling (Figure S3). This consequence illustrated that the performance of the catalyst was maintained well after five recycle uses. The catalyst was expected to be applied in the field of organic wastewater treatment.

3.4. Photocatalytic Performance of Different Pollutants. In order to investigate the applicability of photocatalysts for pollutant degradation, some typical organics were selected as model pollutant. For instance, the tetracycline, rhodamine B, and methyl orange represented antibiotics, cationic, and anionic contaminants, respectively. As illustrated in Figure 7,

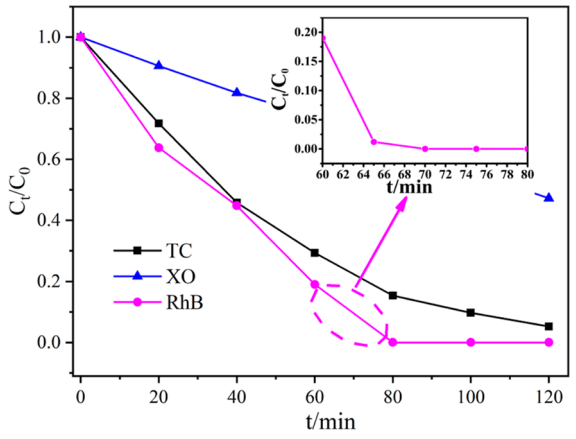

Figure 7. Degradation of different pollutants by UiO-66-NDC/P−C_3N_4.

the degradation efficiencies of UiO-66-NDC/P−C_3N_4 for tetracycline, rhodamine B, and methyl orange solution were 95, 100, and 53% within 120 min, respectively. Especially rhodamine B, it was completely degraded within 65 min. The degradation of methyl orange solution was more difficult, this might be because methyl orange contains an azo (−N═N−) group, and the destruction of this group required higher energy, it was difficult to be oxidized by active free radicals.[43]

A comparative study of UiO-66-NDC/P−C_3N_4 and other photocatalysts previously reported for the photocatalytic hydroxylation of benzene to phenol was conducted, and the results are shown in Table 1. The degradation rate of tetracycline was 95% within 60 min under the photocatalysis of UiO-66-NDC/P−C_3N_4, and the catalytic performance was higher than or comparable with those obtained using other photocatalysts.

3.5. Possible Photocatalytic Mechanisms. *3.5.1. Free Radical Capture Detection of Reactive Substances.* It is well-known that the active species such as $^{\bullet}OH$, h^+, and e^- played a vital role in the photocatalytic degradation.[48] To explore the critical factors in the degradation process, free radical capture experiments were performed. Isopropyl alcohol, potassium dichromate, ascorbic acid, and EDTA-2Na were chosen as to capture agents trap $^{\bullet}OH$, e^-, $^{\bullet}O_2^-$, and h^+, respectively. As illustrated in Figure 8, tetracycline was almost never degraded

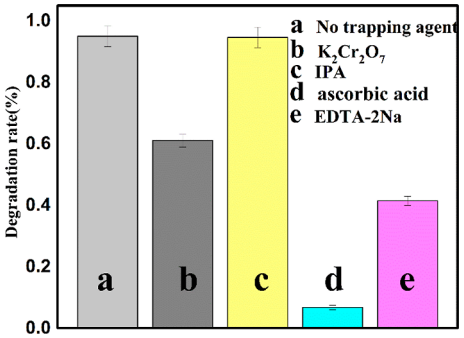

Figure 8. Experimental diagrams of free radical capture of UiO-66-NDC/P−C_3N_4.

in the presence of ascorbic acid, which could react with $^{\bullet}O_2^-$. This result stated that the $^{\bullet}O_2^-$ was the key factor in the degradation. Similarly, the degradation rate of tetracycline was significantly reduced when potassium dichromate, and EDTA-2Na were added to the system. This phenomenon illustrated that the holes (h^+) and electrons (e^-) were another main active substance. However, $^{\bullet}OH$ had almost no effect on the photocatalytic degradation process.

3.5.2. Mechanistic Speculation. The conduction band electric potential value of the UiO-66-NDC/P−C_3N_4 was lower than that of the $O_2/^{\bullet}O_2^-$ (−0.046 eV vs NHE). Under the visible light, photogenerated electrons were easily transferred from P−C_3N_4 through heterojunctions to UiO-66-NDC (as evidenced by XPS results) and reacted with O_2 adsorbed on the material surface to produce superoxide radicals ($^{\bullet}O_2^-$), which, as a highly oxidizing active substance, could not only achieve oxidative degradation of pollutants but also inhibited the complexation of photogenerated electron−hole pairs,[49] The UiO-66-NDC/P−C_3N_4 band gap value Eg obtained from UV−vis DRS curve (Figure 4f) was 2.14 eV, the valence band potential of UiO-66-NDC/P−C_3N_4 could be calculated as 1.78 eV, less than $^{\bullet}OH/OH^-$ REDOX (2.38 eV vs NHE) potential. Therefore, it could be proven that UiO-66-NDC/P−C_3N_4 could not produce hydroxyl radical, which was consistent with

Table 1. Comparison of the Photocatalytic Activity of UiO-66-NDC/P−C_3N_4 with Other Reported Photocatalysts for the Photocatalytic Degradation of Tetracycline

catalyst	amount (mg/mL)	time (min)	concentration	efficiency (%)	refs
$Fe_{0.25}Cu_{0.75}$(BDC)@DE	0.6	120	20 mg/L	93	7
In_2O_3/Co_3O_4@PAL	2	120	50 ppm	80	44
Fe-MILs	0.1	60	25 mg/L	94	45
FOCN-0.45	0.5	60	40 mg/L	92	46
AgI/UiO-66(NH_2)	0.3	40	10 mg/L	66	47
UiO-66-NDC/P−C_3N_4	1	120	30 mg/L	95	this work

https://doi.org/10.1021/acsomega.3c02762
ACS Omega 2023, 8, 27375−27385

the result of the free radical trapping experiment. The generated holes could directly react with the pollutant molecules adsorbed on the catalyst surface to generate carbon dioxide or water which was considered to be a green and environmentally friendly sewage treatment method (Figure 9).[50]

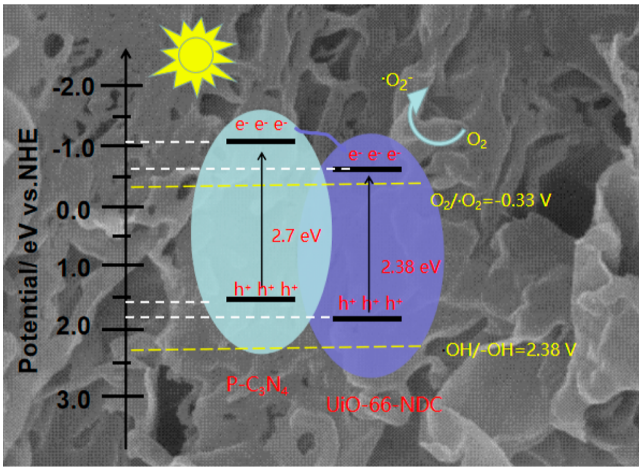

Figure 9. Proposed mechanism of photocatalytic degradation of (TC) by the UiO-66-NDC/P−C_3N_4 under visible light irradiation.

The possible degradation pathway of TC is exhibited in Figure 10. The substance with m/z = 445 represents molecular of TC, and the product P1 can be formed by losing a *N*-methyl in TC molecular. P2 was formed through a dealkylation and dehydration reaction with the action of h^+, and P3 and P4 were formed by further ring-opening and oxidation of product P2. In addition, the products with smaller molecular weight, such as P5, P6, CO_2, and H_2O are released from the reaction.[51,52]

4. CONCLUSIONS

In conclusion, a series of photocatalysts based on the classical Zr-MOF UiO-66 were synthesized by a solvothermal method. All of these catalysts showed satisfying degradation ability for tetracycline under visible light. Therein, the heterojunction UiO-66-NDC/P−C_3N_4 could achieve 95% degradation rate of tetracycline within 120 min which is mainly caused by the $^{\bullet}O_2^-$. Meanwhile, UiO-66-NDC/P−C_3N_4 also showed good degradation ability for other types of dyes, such as rhodamine B and methyl orange. The catalytic performance of the composite was maintained well after five cycles. Therefore, these methods such as incorporating other metals, constructing heterojunctions and taking ligands with a larger conjugated system could improve the catalytic performance of MOFs, which would provide inspiration for the construction of new materials applied in the field of photocatalysis.

ASSOCIATED CONTENT

Supporting Information

The Supporting Information is available free of charge at https://pubs.acs.org/doi/10.1021/acsomega.3c02762.

FTIR spectra characterization of photocatalyst samples, adsorption properties characterization of UIO-66-NDC/P−C_3N_4, and infrared and XRD characterization of UiO-66-NDC/P−C_3N_4 (PDF)

AUTHOR INFORMATION

Corresponding Authors

Liuxue Zhang − *School of Materials and Chemical Engineering, Zhongyuan University of Technology, Zhengzhou 450007, PR China;* orcid.org/0000-0003-0297-037X; Phone: +86-731-62506699; Email: zhanglx@zut.edu.cn; Fax: +86-731-62506095

Shuyan Jiao − *School of Materials and Chemical Engineering, Zhongyuan University of Technology, Zhengzhou 450007, PR China*; Email: jiaosy@zut.edu.cn

Authors

Xu Jia − *School of Materials and Chemical Engineering, Zhongyuan University of Technology, Zhengzhou 450007, PR China*

Fuying Wang − *School of Materials and Chemical Engineering, Zhongyuan University of Technology, Zhengzhou 450007, PR China*

Xuetong Xu − *School of Materials and Chemical Engineering, Zhongyuan University of Technology, Zhengzhou 450007, PR China*

Cong Liu − *School of Materials and Chemical Engineering, Zhongyuan University of Technology, Zhengzhou 450007, PR China*

Genxing Zhu − *School of Materials and Chemical Engineering, Zhongyuan University of Technology, Zhengzhou 450007, PR China*

Xiulian Wang − *School of Energy and Environment, Zhongyuan University of Technology, Zhengzhou 450007, PR China*

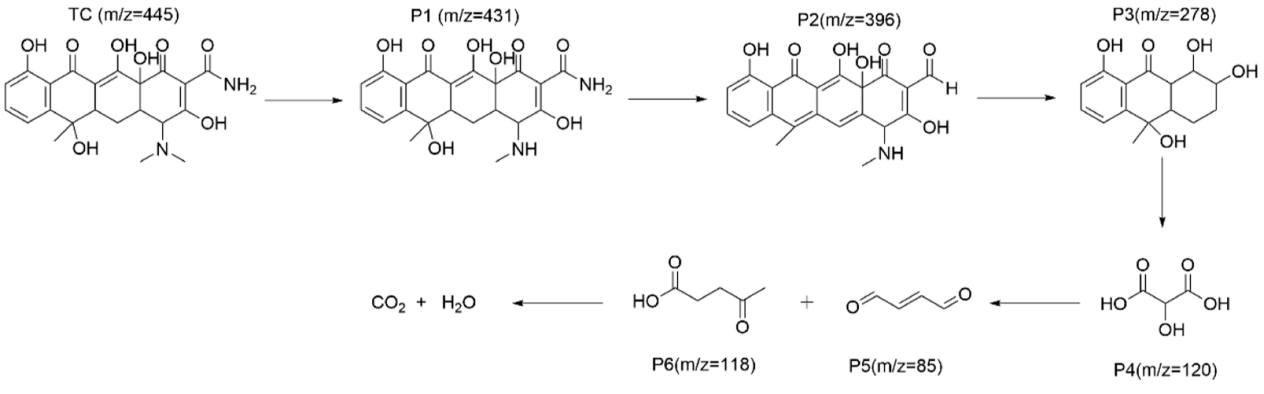

Figure 10. Possible degradation pathway of TC for the UiO-66-NDC/P−C_3N_4.

https://doi.org/10.1021/acsomega.3c02762
ACS Omega 2023, 8, 27375−27385

Guomin Yu − *School of Materials and Chemical Engineering, Zhongyuan University of Technology, Zhengzhou 450007, PR China*

Complete contact information is available at: https://pubs.acs.org/10.1021/acsomega.3c02762

Notes

The authors declare no competing financial interest.

■ ACKNOWLEDGMENTS

This project was financially supported by 2018 Funding Plan for Young Core Teachers of Zhongyuan University of Technology, Discipline Strength Improvement Program of Zhongyuan University of Technology: Program for Cultivating Disciplinary Young Master Supervisor (SD202204), and the Basic Scientific Research Program of Zhongyuan University of Technology (K2018QN018).

■ REFERENCES

(1) Lan, D.; Zhu, H.; Zhang, J.; Li, S.; Chen, Q.; Wang, C.; Wu, T.; Xu, M. Adsorptive removal of organic dyes via porous materials for wastewater treatment in recent decades: A review on species, mechanisms and perspectives. *Chemosphere* **2022**, *293*, 133464.

(2) Liu, H.; Zhang, H.; Dong, X.; Wu, C.; Lichtfouse, E. Removal of antibiotics from black water by a membrane filtration-visible light photocatalytic system. *Journal of Water Process Engineering* **2023**, *53*, 103605.

(3) He, Z.; Xu, X.; Wang, B.; Lu, Z.; Shi, D.; Wu, W. Evaluation of iron-loaded granular activated carbon used as heterogeneous fenton catalyst for degradation of tetracycline. *J. Environ. Manage.* **2022**, *322*, 116077.

(4) Aghapour, A. A.; Alizadeh, N.; Khorsandi, H. Biological degradation and mineralization of tetracycline antibiotic using SBR equipped with a vertical axially rotating biological bed (SBR-VARB). *Biodegradation* **2023**, *34*, 325−340.

(5) Zhang, D.; He, Q.; Hu, X.; Zhang, K.; Chen, C.; Xue, Y. Enhanced adsorption for the removal of tetracycline hydrochloride (TC) using ball-milled biochar derived from crayfish shell. *Colloids Surf., A* **2021**, *615*, 126254.

(6) Zhang, L.; Zheng, Q.; Zhang, Z.; Li, H.; Liu, X.; Sun, J.; Wang, R. Application of Metal−Organic Frameworks (MOFs) in Environmental Biosystems. *Int. J. Mol. Sci.* **2023**, *24* (3), 2145.

(7) Cui, K. P.; He, Y. Y.; Xu, K. J.; Zhang, Y.; Chen, C. B.; Xu, Z. J.; Chen, X. Degradation of Tetracycline Hydrochloride by Cu-Doped MIL-101 (Fe) Loaded Diatomite Heterogeneous Fenton Catalyst. *Nanomaterials* **2022**, *12* (5), 811.

(8) Li, R.; Chen, T.; Lu, J.; Hu, H.; Zheng, H.; Zhu, P.; Pan, X. Metal−organic frameworks doped with metal ions for efficient sterilization: Enhanced photocatalytic activity and photothermal effect. *Water Res.* **2023**, *229*, 119366.

(9) Yulia, F.; Utami, V. J.; Nanda, R.; et al. Preparation of metal-organic frameworks (MOFs) based chromium 2, 6-naphtalenedicarboxylic acid (MIL-101 NDC) for CO_2 adsorption application. In *IOP Conference Series: Materials Science and Engineering*; IOP Publishing, 2021; Vol. *1078*(1), p 012021.

(10) Mohammadnezhad, F.; Kampouri, S.; Wolff, S. K.; Xu, Y.; Feyzi, M.; Lee, J. H.; Ji, X.; Stylianou, K. C. Tuning the optoelectronic properties of hybrid functionalized MIL-125-NH_2 for photocatalytic hydrogen evolution. *ACS Appl. Mater. Interfaces* **2021**, *13* (4), 5044−5051.

(11) Chen, J.; Qin, C.; Mou, Y.; Cao, Y.; Chen, H.; Yuan, X.; Wang, H. Linker regulation of iron-based MOFs for highly effective Fenton-like degradation of refractory organic contaminants. *Chem. Eng. J.* **2023**, *459*, 141588.

(12) He, Y.; Dong, W.; Li, X.; Wang, D.; Yang, Q.; Deng, P.; Huang, J. Modified MIL-100 (Fe) for enhanced photocatalytic degradation of tetracycline under visible-light irradiation. *J. Colloid Interface Sci.* **2020**, *574*, 364−376.

(13) Wang, C. C.; Yi, X. H.; Wang, P. Powerful combination of MOFs and C_3N_4 for enhanced photocatalytic performance. *Appl. Catal., B* **2019**, *247*, 24−48.

(14) Bai, Y.; Dou, Y.; Xie, L. H.; Rutledge, W.; Li, J. R.; Zhou, H. C. Zr-based metal−organic frameworks: design, synthesis, structure, and applications. *Chem. Soc. Rev.* **2016**, *45* (8), 2327−2367.

(15) Qiao, X.; Liu, Y.; Yang, Y.; Wang, H.; Ma, J.; Wang, D.; Gao, N.; Li, L.; Liu, W.; Wang, H. Synthesis optimization of metal-organic frameworks MIL-125 and its adsorption separation on C_8 aromatics measured by Pulse Test and simulation calculation. *J. Solid State Chem.* **2021**, *296*, 121956.

(16) Han, Y.; Zhai, J.; Zhang, L.; Dong, S. Direct carbonization of cobalt-doped NH_2-MIL-53(Fe) for electrocatalysis of oxygen evolution reaction. *Nanoscale* **2016**, *8* (2), 1033−1039.

(17) Ong, W.-J.; Tan, L.-L.; Ng, Y. H.; Yong, S.-T.; Chai, S.-P. Carbon nitride (g-C_3N_4)-based photocatalysts for artificial photosynthesis and environmental remediation: are we a step closer to achieving sustainability. *Chem. Rev.* **2016**, *116*, 7159−7329.

(18) Tang, J.; Zhang, T.; Zhang, Q.; Duan, Z.; Li, C.; Hou, D.; Xv, Q.; Meng, C.; Zhang, Y.; Zhu, Y. In-situ growth UiO-66 on Bi_2O_3 to fabrication p-p heterojunction with enhanced visible-light degradation of tetracycline. *J. Solid State Chem.* **2021**, *302*, 122353.

(19) Mehrabanpour, N.; Nezamzadeh-Ejhieh, A.; Ghattavi, S.; Ershadi, A. A magnetically separable clinoptilolite supported CdS-PbS photocatalyst: Characterization and photocatalytic activity toward cefotaxime. *Appl. Surf. Sci.* **2023**, *614*, 156252.

(20) Wang, L.; Dai, X.; Man, Z.; Li, J.; Jiang, Y.; Liu, D.; Xiao, H.; Shah, S. Dynamics and treatability of heavy metals in pig farm effluent wastewater by using UiO-66 and UiO-66-NH_2 nanomaterials as adsorbents. *Water, Air, Soil Pollut.* **2021**, *232* (7), 294.

(21) Zamani, S.; Abbasi, A.; Masteri-Farahani, M.; Rayati, S. One-pot, facile synthesis and fast separation of a UiO-66 composite by a metalloporphyrin using nanomagnetic materials for oxidation of olefins and allylic alcohols. *New J. Chem.* **2022**, *46* (2), 654−662.

(22) Butova, V. V.; Budnyk, A. P.; Charykov, K. M.; Vetlitsyna-Novikova, K. S.; Bugaev, A. L.; Guda, A. A.; Damin, A.; Chavan, S. M.; Øien-Ødegaard, S.; Lillerud, K. P.; et al. Partial and complete substitution of the 1, 4-benzenedicarboxylate linker in UiO-66 with 1, 4-naphthalenedicarboxylate: synthesis, characterization, and H_2-adsorption properties. *Inorg. Chem.* **2019**, *58* (2), 1607−1620.

(23) Schelling, M.; Otal, E.; Kim, M.; Hinestroza, J. P. Conformal functionalization of cotton fibers via isoreticular expansion of UiO-66 metal-organic frameworks. *Coatings* **2020**, *10* (12), 1172.

(24) Zhang, Y.; Song, X.; Li, S.; Zhao, B.; Tong, L.; Wang, Y.; Li, Y. Two-step preparation of Keggin-PW_{12}@UiO-66 composite showing high-activity and long-life conversion of soybean oil into biodiesel. *RSC Adv.* **2021**, *11* (60), 38016−38025.

(25) Jilani, A.; Hussain, S. Z.; Ansari, M. O.; Kumar, R.; Dustgeer, M. R.; Othman, M. H. D.; Barakat, M. A.; Melaibari, A. A. Facile synthesis of silver decorated reduced graphene oxide@zinc oxide as ternary nanocomposite: an efficient photocatalyst for the enhanced degradation of organic dye under UV-visible light. *J. Mater. Sci.* **2021**, *56* (12), 7434−7450.

(26) Zhang, N.; Ejtemaei, M.; Nguyen, A. V.; Zhou, C. XPS analysis of the surface chemistry of sulfuric acid-treated kaolinite and diaspore minerals with flotation reagents. *Miner. Eng.* **2019**, *136*, 1−7.

(27) Li, Z.; Zhang, Z.; Dong, Z.; Wu, Y.; Liu, J.; Cheng, Z.; Liu, Y.; Wang, Y.; Zheng, Z.; Cao, X.; et al. Synthesis of MoS_2/P-g-C_3N_4 nanocomposites with enhanced visible-light photocatalytic activity for the removal of Uranium(VI). *J. Solid State Chem.* **2021**, *302*, 122305.

(28) Xu, X.; Liu, R.; Cui, Y.; Liang, X.; Lei, C.; Meng, S.; Ma, Y.; Lei, Z.; Yang, Z. PANI/FeUiO-66 nanohybrids with enhanced visible-light promoted photocatalytic activity for the selectively aerobic oxidation of aromatic alcohols. *Appl. Catal., B* **2017**, *210*, 484−494.

(29) Wang, C. Y.; Zhang, Y. J.; Wang, W. K.; Pei, D. N.; Huang, G. X.; Chen, J. J.; Zhang, X.; Yu, H. Q. Enhanced photocatalytic

degradation of bisphenol A by Co-doped BiOCl nanosheets under visible light irradiation. *Appl. Catal., B* **2018**, *221*, 320−328.
(30) Xu, X.; Deng, F.; Shao, P.; Dionysiou, D. D.; Luo, X.; Li, X.; Zhang, S.; Liu, X.; Liu, M. Internal electric field driving separation and migration of charge carriers via Z-scheme path in $AgIn_5S_8$/ZnO heterojunction for efficient decontamination of pharmaceutical pollutants. *Chem. Eng. J.* **2022**, *428*, 132096.
(31) Mu, Y.; Xie, Y. Theoretical and experimental comparison of electrical properties of nickel (II) coordinated and protonated polyaniline. *J. Phys. Chem. C* **2019**, *123* (30), 18232−18239.
(32) Samanta, S.; Yadav, R.; Kumar, A.; Kumar Sinha, A.; Srivastava, R. Surface modified C, O co-doped polymeric g-C_3N_4 as an efficient photocatalyst for visible light assisted CO_2 reduction and H_2O_2 production. *Appl. Catal., B* **2019**, *259*, 118054.
(33) Larijani, R. S.; Ghadiri, M.; Hafezi, M.; Jafarikojour, M.; Dabir, B. Evaluation of mass and photon transfer enhancement by an impinging jet atomization photoreactor for photocatalytic degradation of p-nitrophenol. *J. Photochem. Photobiol., A* **2021**, *408*, 113088.
(34) Shen, Q.; Wei, L.; Bibi, R.; Wang, K.; Hao, D.; Zhou, J.; Li, N. Boosting photocatalytic degradation of tetracycline under visible light over hierarchical carbon nitride microrods with carbon vacancies. *J. Hazard. Mater.* **2021**, *413*, 125376.
(35) Li, M.; Li, Y. W.; Yu, P. F.; Zhao, H. M.; Xiang, L.; Feng, N. X.; Li, Q. K.; He, K. Y.; Luo, X.; Cai, Q. Y.; et al. Exploring degradation mechanism of tetracycline via high-effective peroxymonosulfate catalysts of montmorillonite hybridized CoFe composites and safety assessment. *Chem. Eng. J.* **2022**, *427*, 130930.
(36) Murillo-Sierra, J. C.; Hernández-Ramírez, A.; Zhao, Z. Y.; Martínez-Hernández, A.; Gracia-Pinilla, M. Construction of direct Z-scheme WO_3/ZnS heterojunction to enhance the photocatalytic degradation of tetracycline antibiotic. *J. Environ. Chem. Eng.* **2021**, *9* (2), 105111.
(37) Kumar Palaniswamy, V.; Ramasamy, B.; Manoharan, K.; Raman, K.; Sundaram, R. Enhanced photocatalytic degradation of tetracycline antibiotic using m-$BiVO_4$ photocatalyst under visible light irradiation. *Chem. Phys. Lett.* **2021**, *771* (9), 138531.
(38) Wang, G.; Chen, Q.; Liu, Y.; Ma, D.; Xin, Y.; Ma, X.; Zhang, X. In situ synthesis of graphene/WO_3 co-decorated TiO_2 nanotube array photoelectrodes with enhanced photocatalytic activity and degradation mechanism for dimethyl phthalate. *Chem. Eng. J.* **2018**, *337*, 322−332.
(39) Zhang, B.; He, X.; Yu, C.; Liu, G.; Ma, D.; Cui, C.; Yan, Q.; Zhang, Y.; Zhang, G.; Ma, J.; et al. Degradation of tetracycline hydrochloride by ultrafine TiO_2 nanoparticles modified g-C_3N_4 heterojunction photocatalyst: Influencing factors, products and mechanism insight. *Chin. Chem. Lett.* **2022**, *33* (3), 1337−1342.
(40) Eskandarloo, H.; Badiei, A.; Behnajady, M. A. Study of the effect of additives on the photocatalytic degradation of a triphenylmethane dye in the presence of immobilized TiO_2/NiO nanoparticles: artificial neural network modeling. *Ind. Eng. Chem. Res.* **2014**, *53* (17), 6881−6895.
(41) Huang, L.; Sun, Y.; Wang, W.; Yue, Q.; Yang, T. Comparative study on characterization of activated carbons prepared by microwave and conventional heating methods and application in removal of oxytetracycline (OTC). *Chem. Eng. J.* **2011**, *171* (3), 1446−1453.
(42) Li, Z.; Li, H.; Zeng, X.; Liu, S.; Yang, Y. Adsorption and photodegradation of tetracycline by mannose-grafted chitosan composite films: performance, mechanism and availability. *Chem. Eng. J.* **2023**, *458*, 141455.
(43) Xu, R.; Su, M.; Liu, Y.; Chen, Z.; Ji, C.; Yang, M.; Chang, X.; Chen, D. Comparative study on the removal of different-type organic pollutants on hierarchical tetragonal bismutite microspheres: adsorption, degradation and mechanism. *J. Clean. Prod.* **2020**, *242*, 118366.
(44) Xu, J.; Gao, J.; Liu, Y.; Li, Q.; Wang, L. Fabrication of In_2O_3/Co_3O_4-palygorskite composites by the pyrolysis of In/Co-MOFs for efficient degradation of methylene blue and tetracycline. *Mater. Res. Bull.* **2017**, *91*, 1−8.
(45) Chen, H.; Cai, T.; Dong, W.; Wang, J.; Liu, Y.; Li, W.; Xia, X.; Tang, L. Catalytic thermal degradation of tetracycline based on iron-based MOFs and annealed derivative in dark condition. *J. Clean. Prod.* **2023**, *406*, 136976.
(46) Guo, T.; Wang, K.; Zhang, G.; Wu, X. A novel α-Fe_2O_3@g-C_3N_4 catalyst: synthesis derived from Fe-based MOF and its superior photo-Fenton performance. *Appl. Surf. Sci.* **2019**, *469*, 331−339.
(47) Pan, Y.; Yuan, X.; Jiang, L.; Wang, H.; Yu, H.; Zhang, J. Stable self-assembly AgI/UiO-66 (NH_2) heterojunction as efficient visible-light responsive photocatalyst for tetracycline degradation and mechanism insight. *Chem. Eng. J.* **2020**, *384*, 123310.
(48) Al-Namshah, K. S.; Mariappan, S. M.; Shkir, M.; Hamdy, M. S. Photocatalytic degradation mechanism of Ce-loaded ZnO catalysts toward methyl green dye pollutant. *Appl. Phys. A: Mater. Sci. Process.* **2021**, *127* (6), 452.
(49) Wang, Z.; Jia, H.; Liu, Z.; Peng, Z.; Dai, Y.; Zhang, C.; Guo, X.; Wang, T.; Zhu, L. Greatly enhanced oxidative activity of δ-MnO_2 to degrade organic pollutants driven by dominantly exposed {−111} facets. *J. Hazard. Mater.* **2021**, *413*, 125285.
(50) Liou, S. Y.; Dodd, M. C. Evaluation of hydroxyl radical and reactive chlorine species generation from the superoxide/hypochlorous acid reaction as the basis for a novel advanced oxidation process. *Water Res.* **2021**, *200* (10), 117142.
(51) Sun, H.; Guo, F.; Pan, J.; Huang, W.; Wang, K.; Shi, W. One-pot thermal polymerization route to prepare N-deficient modified g-C_3N_4 for the degradation of tetracycline by the synergistic effect of photocatalysis and persulfate-based advanced oxidation process. *Chem. Eng. J.* **2021**, *406*, 126844.
(52) Xiong, J.; Xu, H.; Yin, X.; Yang, B.; Petropoulos, E.; Xue, L.; Yang, L.; He, S. Visible-light driven Tetracycline hydrochloride degradation by Nano-lanthanum hydroxide modified carbon nitride: performance, mechanism, and application in real wastewater treatment. *Environ. Sci.: Water Res. Technol.* **2023**, DOI: 10.1039/D3EW00233K.

https://doi.org/10.1021/acsomega.3c02762
ACS Omega 2023, 8, 27375−27385